Supplementary Material

CHD_3 Dissociation on Pt(111): A Comparison of the Reaction Dynamics Based on the PBE Functional and on a Specific Reaction Parameter Functional

H. Chadwick[a),b)], D. Migliorini[a)] and G.J. Kroes

Leiden Institute of Chemistry, Gorlaeus Laboratories, Leiden University, P.O. Box 9502, 2300 RA Leiden, The Netherlands

a) H. Chadwick and D. Migliorini contributed equally to this work

b) Email: h.j.chadwick@lic.leidenuniv.nl

SI. Pseudopotentials

All the calculations reported in this work have been performed using the 2005 version of the platinum PBE PAW pseudopotentials for VASP. However, the surfaces used as initial conditions for the AIMD scattering simulations with the PBE functional have been equilibrated previously in the group with an older version (i.e., from 2001) of the same pseudopotentials. For clarity's sake from now on these pseudopotentials will be referred to as paw2005 and paw2001, respectively. This choice is justified by the similarity of the two different pseudopotentials and the resulting barrier heights computed with them. Both the pseudopotentials have a {[Xe] $4f^{14}$} core that treat explicitly 10 valence electrons (i.e., $5d^9$ $6s^1$). Here we address the question of whether the use of different pseudopotentials as pointed out could have led to large systematic errors.

The Pt(111) slab has been optimized and the barrier computed with the two pseudopotentials, the results from which are reported in Table SI. The difference in the bulk lattice constant is 0.008 Å while the difference in the 500 K surface lattice constant is 0.006 Å, amounting to a difference in cell size for the 3x3 cell used in the AIMD of 0.018 Å. The computed barrier heights are the same within 0.1 kJ/mol.

The AIMD scattering calculations for PBE have been propagated using paw2005, however the slabs have been optimized and equilibrated with paw2001. This implies that the surface lattice constant in the AIMD trajectories is the one computed with paw2001 but the trajectories are carried out with paw2005. This could introduce stress on the slab leading to a change in the interlayer distances. Therefore the interlayer spacing has been recomputed using paw2005 but for a slab generated from the bulk lattice constant optimized with paw2001. The results, reported in Table SII, show a maximum difference of 0.006 Å from the paw2005 setup.

As an additional test, the slab generated from the paw2001 lattice constant and relaxed using paw2005 has been used to compute the transition state (TS) for the CH_4 dissociation using the paw2005 pseudopotentials. This system, which should be the one that best represents the conditions

in the AIMD simulations, shows a barrier of 77.7 kJ/mol which is only 0.3 kJ/mol lower than the one computed consistently with paw2005 (i.e., 78.0 kJ/mol) and only 0.4 kJ/mol lower than the one computed consistently with paw2001 (i.e., 78.1 kJ/mol[1]). This suggests that the dynamics we performed are sufficiently reliable and sufficiently accurate for the purpose of this work, as the energy spacing reported between the PBE and SRP32-vdW reaction probability curves in the main paper (13.9 kJ/mol) is more than an order of magnitude larger than the differences in barrier heights reported here.

SII. Analysis of the shape of the potential energy surfaces

The minimum energy paths (MEPs) across the two dimensional SRP32-vdW and PBE potential energy surfaces (PESs) presented in Fig. 5 are reproduced in Fig. S1A in blue and green, respectively. The red points correspond to the transition states, and the black points to the 'elbow', i.e. the point on the MEP where the curvature is the highest. The curvature was determined by fitting 3 adjacent points on the MEP to a circle, and then computing the curvature as 1/radius. As shown in Table SIII and Figure S1B the curvature for the two PESs is similar, although it is slightly higher for the SRP32-vdW PES meaning the turn in the MEP is slightly tighter. The positions of the TS on the MEP as determined from the two dimensional PES, which are also shown in Table SIII, are in good agreement with the geometries of the saddle points presented in Table II of the manuscript, which were determined using the dimer method[2,3].

One dimensional cuts through the two dimensional PESs at the transition state along the vector perpendicular to the two dimensional MEP (along χ) are presented in Fig. S2. The curves have been shifted down by the activation barrier so that the saddle point is at 0 kJ/mol to allow the width of the saddle points for the SRP32-vdW (blue) and PBE (green) functionals to be compared. The saddle point for the SRP32-vdW functional is slightly wider than for the PBE functional.

The distributions of where the reacted trajectories cross the vector perpendicular to the MEP at the transition state (χ_r) is shown for the SRP32-vdW (blue) and PBE (green) functionals in Fig.

S3 for trajectories that start within 0.1 Å (A), 0.2 Å (B), 0.3 Å (C) and 0.4 Å (D) of a top site in the xy plane. χ_r is calculated using Eq. (6) and is 0 Å at the transition state. The distributions were obtained using Gaussian binning with a 0.005 Å bin size and a 0.02 Å broadening parameter. For the reactive trajectories that start within 0.1 Å of the top site, where the PES is most reliable (the two dimensional PESs in Fig. 5 were computed for the TS which is at the top site), there is some evidence for the SRP32-vdW trajectories crossing the vector at more negative values of χ than the PBE trajectories, although this is not seen for trajectories that react further from the top site. This suggests that the faster SRP32-vdW trajectories do not sample the repulsive part of the PES more than the PBE trajectories due to the 'bobsled effect' [4–6].

SIII. Comparison of properties averaged over trajectories

For the PBE functional 7100 trajectories were run (3600 laser-off and 3500 for $v_1 = 1$) and for the SRP32-vdW functional 7000 trajectories were run (4000 laser-off and 3000 for $v_1 = 1$). Tables SIV and SV present the average of several parameters for the trajectories that react and scatter respectively, for the two functionals. The property of interest has first been averaged for a single collision energy, and then averaged over collision energy to remove any errors associated with different numbers of trajectories being run and analysed for the PBE and SRP32-vdW functionals. The width (σ) of the distributions has been found using

$$\sigma = \sqrt{\frac{\sum_N (x_N - \langle x \rangle)^2}{(N-1)}} \quad \text{(S1)}$$

where $\langle x \rangle$ is the average, and the error (σ_M) using

$$\sigma_M = \frac{\sigma}{\sqrt{N}} \quad \text{(S2)}$$

where N is the number of trajectories that react or scatter.

For the reacted trajectories (Table SIV), some differences can be seen in the angular distributions. For the SRP32-vdW trajectories, a larger change in the angle ($\delta\theta$) between the dissociating bond and the surface normal (θ) is seen than in the PBE trajectories, suggesting the

molecule has to reorient more to react. However, the change in the angle ($\delta\beta$) between the dissociating bond and umbrella axis of the CHD_3 (β) is smaller for the SRP32-vdW functional. The distributions of both of these angles for the molecules that react are slightly wider for the PBE functional than the SRP32-vdW functional, which suggests that PBE trajectories can react in slightly less favored geometries than the SRP32-vdW functional which would increase the reactivity of the PBE trajectories compared to the SRP32-vdW trajectories.

The other significant difference seen between the reacted trajectories for the two functionals in Table SIV is that the puckering of the surface is larger for the SRP32-vdW functional than the PBE functional. Both the height of the atom above which the methane dissociates ($Z_{\mathrm{d}}^{\mathrm{rxn}}$) and the average height of all the atoms in the first layer of the surface ($\langle Z_{\mathrm{d}} \rangle$) is bigger for the SRP32-vdW functional, and the difference for $Z_{\mathrm{d}}^{\mathrm{rxn}}$ is significant. Using the fits in Fig. 4 gives an activation barrier height of 75.5 kJ/mol for the PBE functional and 72.4 kJ/mol for the SRP32-vdW functional with the surface atom at the values of $Z_{\mathrm{d}}^{\mathrm{rxn}}$ presented in Table SIV. This suggests that the reactivity of the SRP32-vdW trajectories is limited by other dynamical factors.

The average properties of the scattered trajectories are presented in Table SV. The most significant difference between the two functionals is the energy transferred to the surface (δE_{surf}), which can be attributed to the presence of the van der Waals well in the SRP32-vdW trajectories as discussed in the main manuscript. The vibrational energy change (δE_{vib}) of the scattered molecules is the same for the two functionals, suggesting that the van der Waals well does not lead to surface mediated energy transfer from translational energy to vibrational energy in the reactive trajectories. Therefore, the larger surface puckering found for the SRP32-vdW reacted trajectories could well be due to reaction being more difficult as a result of other dynamical factors.

REFERENCES

[1] F. Nattino, D. Migliorini, M. Bonfanti, and G.J. Kroes, J. Chem. Phys. **144**, 44702 (2016).

[2] G. Henkelman and H. Jónsson, J. Chem. Phys. **111**, 7010 (1999).

[3] A. Heyden, A.T. Bell, and F.J. Keil, J. Chem. Phys. **123**, 224101 (2005).

[4] E.A. McCullough and R.E. Wyatt, J. Chem. Phys. **51**, 1253 (1969).

[5] R.A. Marcus, J. Chem. Phys. **45**, 4493 (1966).

[6] R.D. Levine, *Molecular Reaction Dynamics* (Cambridge University Press, Cambridge, 2005).

TABLE SI. Comparison between the slabs optimized with paw2001 and with paw2005 pseudopotentials. In the table the bulk lattice constant, the surface lattice constant for the AIMD cell including the thermal expansion for Pt at 500 K, the interlayer spacing and the barrier heights are reported. Note that in the table the barriers reported have been computed consistently with the pseudopotentials used for the slab optimization.

Observable	Functional	paw2001	paw2005	Difference
bulk lattice constant (Å)	PBE	3.97479	3.96652	0.00827
500 K surface lattice constant (Å)	PBE	2.82144	2.81557	0.00587
interlayer distance #1 (Å)	PBE	2.31645	2.31010	0.00635
interlayer distance #2 (Å)	PBE	2.28154	2.27378	0.00776
interlayer distance #3 (Å)	PBE	2.28154	2.27377	0.00777
interlayer distance #4 (Å)	PBE	2.31645	2.31007	0.00638
Barrier height (kJ/mol)	PBE	78.1	78.0	0.1

TABLE SII. Interlayer spacing and activation barrier height computed for the slabs optimized and relaxed consistently with the same pseudopotentials and for the mixed setup closest to the one used in the AIMD scattering calculations (last row).

Pseudopotential used for bulk lattice constant	Pseudopotential used for interlayer spacing	Interlayer #1 (Å)	Interlayer #2 (Å)	Barrier height (kJ/mol)
paw2001	paw2001	2.31645	2.28154	78.0
paw2005	paw2005	2.31010	2.27378	78.1
paw2001	paw2005	2.30435	2.26734	77.7

TABLE SIII. The position of the maximum radius of curvature, the maximum radius of curvature and the position on the transition state in the two dimensional minimum energy paths shown in Fig. 5 and Fig. S1A for the PBE and the SRP32-vdW functional.

Functional	r (Å)	Z (Å)	Curvature (1/Å)	r^{TS} (Å)	Z_C^{TS} (Å)
PBE	1.270	2.314	5.3	1.50	2.24
SRP32-vdW	1.260	2.353	5.6	1.53	2.26

TABLE SIV. The average, width and error calculated for the trajectories that react for various distributions of several properties listed below the table for the PBE and the SRP32-vdW functionals.

	PBE			SRP32-vdW		
	Average	σ	σ_M	Average	σ	σ_M
E_{kin} (kJ/mol)	9.8	11.9	1.4	9.8	12.9	2.2
θ_{i} (˚)	132.0	19.4	2.4	133.9	18.3	3.1
θ_{f} (˚)	125.2	9.7	1.2	124.1	10.2	1.8
$\delta\theta$ (˚)	-6.8	18.1	2.2	-9.8	15.7	2.6
β_{i} (˚)	131.5	20.2	2.5	134.2	19.3	3.2
β_{f} (˚)	150.4	12.5	1.6	149.5	12.2	2.1
$\delta\beta$ (˚)	18.9	22.0	2.7	15.3	19.3	3.3
γ_{i} (˚)	13.6	6.9	0.9	13.2	6.7	1.1
γ_{f} (˚)	33.8	12.7	1.6	32.9	13.0	2.2
$\delta\gamma$ (˚)	20.2	14.5	1.8	19.7	14.5	2.5
δ_{COM} (Å)	0.086	0.057	0.007	0.066	0.048	0.009
$Z_{\mathrm{d}}^{\mathrm{rxn}}$(Å)	0.052	0.111	0.014	0.107	0.114	0.019
$E_b(Z_{\mathrm{d}}^{\mathrm{rxn}})$ (kJ/mol)	75.5	-	-	72.4	-	-
$\langle Z_{\mathrm{d}} \rangle$ (Å)	0.017	0.057	0.007	0.061	0.047	0.008
δ_{Top} (Å)	0.573	0.266	0.033	0.575	0.279	0.047

E_{kin} Kinetic energy at the point where the dissociating bond becomes larger than the TS value
θ_{i} Angle between the dissociating bond and surface normal at the start of the trajectory
θ_{f} Angle between the dissociating bond and surface normal at the point where it becomes larger than the TS value
$\delta\theta$ Change in θ
β_{i} Angle between the umbrella axis and surface normal at the start of the trajectory
β_{f} Angle between the umbrella axis and surface normal at the point where the dissociating bond becomes larger than the TS value
$\delta\beta$ Change in β
γ_{i} Angle between the umbrella axis and the bond that dissociates at the start of the trajectory
γ_{f} Angle between the umbrella axis and dissociating bond at the point where the dissociating bond becomes larger than the TS value
$\delta\gamma$ Change in γ
δ_{COM} Change in xy position of the COM between the start of the trajectory and the point of reaction
$Z_{\mathrm{d}}^{\mathrm{rxn}}$ Height of the surface atom above which the dissociation occurs
$E_b(Z_{\mathrm{d}}^{\mathrm{rxn}})$ Activation barrier at the height of the surface atom above which dissociation occurs
$\langle Z_{\mathrm{d}} \rangle$ Average height of the atoms in the top layer of the surface when the dissociation occurs
δ_{Top} Distance in the xy plane of the COM from a top site when the reaction occurs

TABLE SV. The average, width and error calculated for the scattered trajectories for various distributions of several properties listed below the table for the PBE and the SRP32-vdW functionals.

	PBE			SRP32-vdW		
	Average	σ	σ_M	Average	σ	σ_M
$E_{\mathrm{rot}}^{\mathrm{i}}$ (kJ/mol)	0.034	0.045	0.002	0.033	0.044	0.002
$E_{\mathrm{rot}}^{\mathrm{c}}$ (kJ/mol)	3.1	4.4	0.2	2.8	4.3	0.2
$E_{\mathrm{vib}}^{\mathrm{i}}$ (kJ/mol)	107.7	7.6	0.4	107.6	6.9	0.3
$E_{\mathrm{vib}}^{\mathrm{f}}$(kJ/mol)	114.4	13.5	0.6	114.3	12.9	0.6
δE_{vib} (kJ/mol)	6.6	11.1	0.5	6.7	10.8	0.5
δ_{COM} (Å)	0.064	0.041	0.002	0.053	0.030	0.001
δE_{surf} (kJ/mol)	-14.8	10.2	0.5	-16.4	12.4	0.5

$E_{\mathrm{rot}}^{\mathrm{i}}$ Rotational energy at the start of the trajectory
$E_{\mathrm{rot}}^{\mathrm{c}}$ Rotational energy at the distance of closest approach
$E_{\mathrm{vib}}^{\mathrm{i}}$ Vibrational energy at the start of the trajectory
$E_{\mathrm{vib}}^{\mathrm{f}}$ Vibrational energy at the end of the trajectory
δE_{vib} Change in vibrational energy
δ_{COM} Change in xy position of the COM between the start of the trajectory and at the distance of closest approach
δE_{surf} Energy transfer to the surface

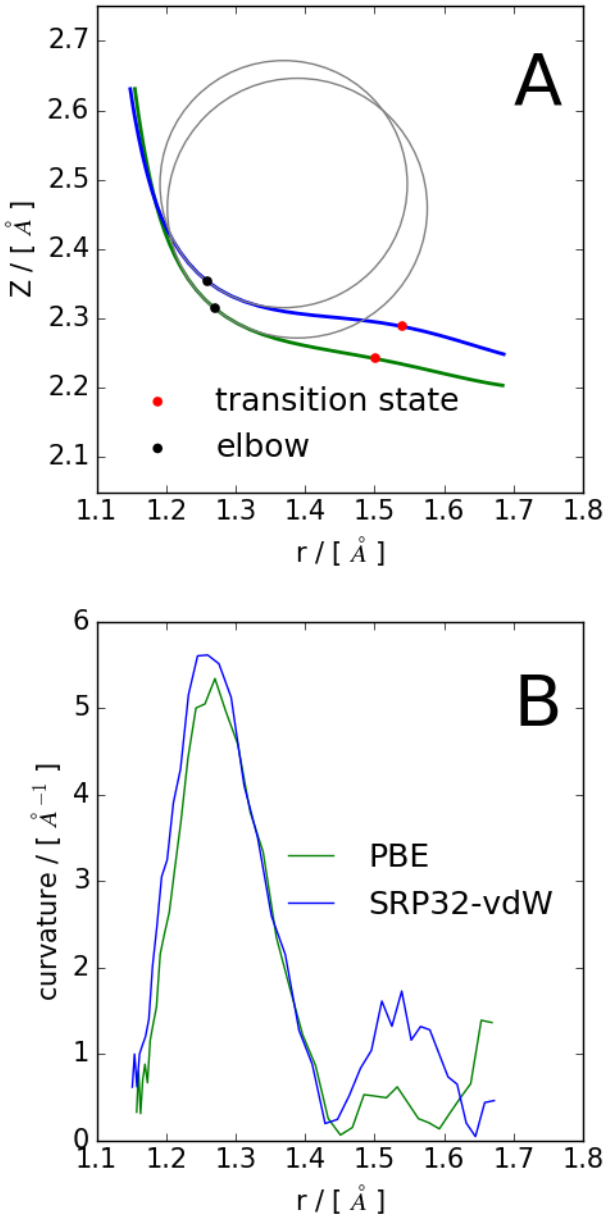

FIG S1. Panel A. The minimum energy path across the two dimensional cuts through the potential energy surfaces presented in Fig. 5 for the PBE (green) and the SRP32-vdW (blue) functionals. The black points show the part of the curve with the maximum curvature, and the red points the transition states. Panel B. The curvature of the minimum energy path for the two functionals.

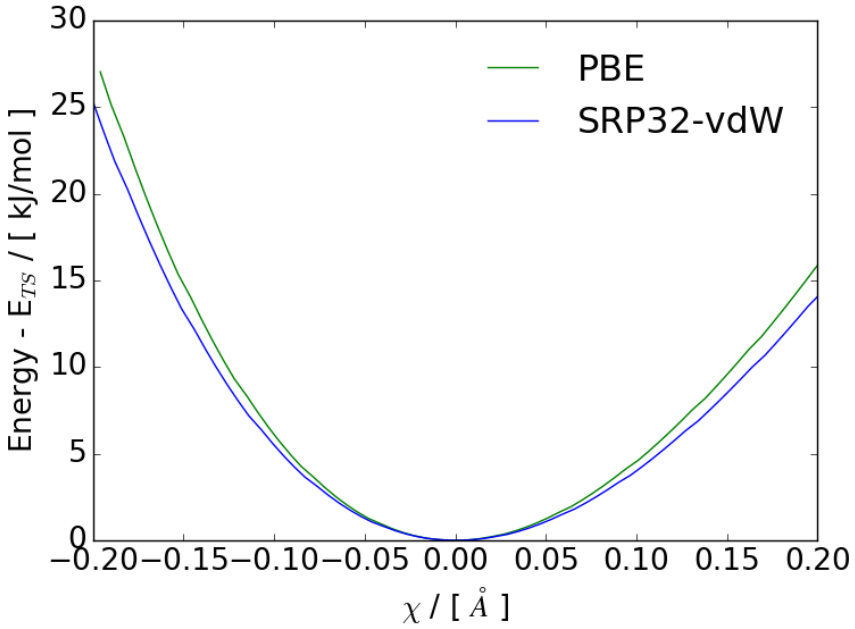

FIG S2. The variation in the potential energy surface perpendicular to the minimum energy path at the transition state presented in Fig. 5 for the PBE functional (green) and the SRP32-vdW functional (blue).

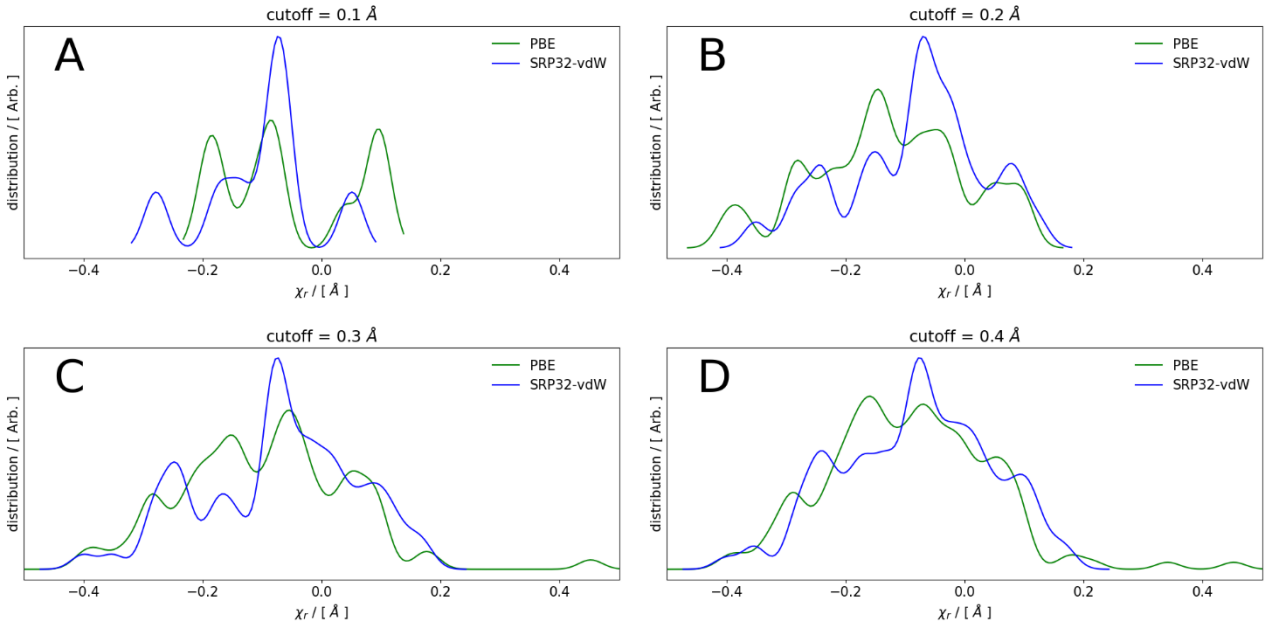

FIG S3. The distributions of the distance between the saddle point to the point where the reacted trajectories cross the vector perpendicular to the minimum energy path (χ_r) for the PBE (green) and SRP32-vdW (blue) trajectories that start within 0.1 Å (A) 0.2 Å (B), 0.3 Å (C) and 0.4 Å (D) of a top site on the Pt(111) surface.